Designing and building Si bolometers for diagnostics and spectroscopy of magnetically trapped hydrogen gas

Master's thesis
University of Turku
Department of Physics
and Astronomy
Physics
2020
Otto Hanski
Supervisors:
Adj. prof. Sergey Vasiliev
doc. Jarno Järvinen

The originality of this thesis has been checked in accordance with the University of Turku quality assurance system using the Turnitin OriginalityCheck service.

UNIVERSITY OF TURKU
Department of Physics and Astronomy

HANSKI, OTTO: Designing and building Si bolometers for diagnostics and spectroscopy of magnetically trapped hydrogen gas

Master's thesis, 44 p., 3 appendix p.
Physics
2020

In this thesis we will be discussing the theory behind low-temperature bolometers for measurements of atomic hydrogen, as well as the possibility of building such bolometers from affordable commercially available silicon wafers, based on previous research into the low-temperature properties of doped silicon.

Additionally experiments conducted over the summer of 2020 to find a proper silicon material for such bolometers will be presented along with sensitivity comparison to previously used sensors.

Keywords: Silicon, Bolometer, Variable Range Hopping, Magnetic trapping, Atomic hydrogen

Contents

1 Introduction

The Hydrogen Research Group at the University of Turku is currently working on a magnetic trap for atomic hydrogen. For this magnetic trap it is required to build sensors for the purpose of diagnostics, as we need to know how much hydrogen gas we have managed to trap and how well we can retain that gas. For this we are planning to use bolometers to detect the recombination of atomic hydrogen into molecules, which releases 4.6 eV per recombination event. At a later point in the experiments, the bolometers could also be used for spectroscopy of our hydrogen sample with a planned UV laser system.

Silicon bolometers have the advantage of being extremely sensitive, while being relatively cheap to construct. With the proper doping concentration, one may achieve a difference in resistance of three to four orders of magnitude in the measurement range. By changing the size of the sensor, we can adjust the thermal capacity and therefore the thermal response of our sensor. With a small enough sensor, it should be possible to detect even a single hydrogen recombination event, or a single UV photon.

2 Theoretical background

2.1 On the magnetic trap project

For properly designing a sensor for an experiment, it is of course important to understand the purpose and specifics of the experiment the sensor is meant for. In this case, the primary purpose of the bolometers is spectroscopy and diagnostics of spin-polarized atomic hydrogen trapped in the Ioffe-Pritchard magnetic trap built by the Hydrogen Research Group at the University of Turku. The magnetic trap was designed as an octupole system of racetrack coils for radial confinement of hydrogen atoms, and pinch coils at top and bottom for confinement along the axis of the

magnet (see fig. 1).

In an Ioffe-Pritchard trap, as originally proposed by David Pritchard in his publication in 1983 [1], the basic idea is using a multipole (in our case, octupole) magnet to create a magnetic field that has a local minimum at the center formed by the fields canceling out at the middle, creating a potential well to capture low-field seeking hydrogen atoms (denoted H↓). It's worth noting that it's impossible to create a field maximum in a current-free space that would instead trap high-field seekers [1].

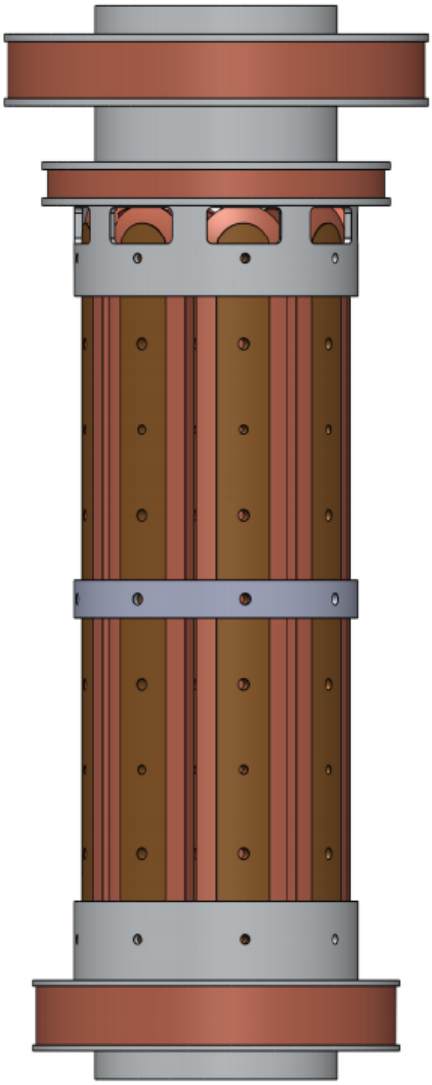

Figure 1: A picture showing the design of the magnetic trap. Note the racetracks of the octupole, and the sets of pinch coils at top and bottom.

The magnetic trap will be used to capture H↓ for experiments, with the purpose of studying the fundamental properties of hydrogen. The experiment is designed after the previous experiments conducted at MIT [2], where Bose-Einstein condensation (BEC) was first observed in atomic hydrogen. The setup in Turku will also be able to generate BEC of hydrogen, for the first time since the initial measurements at MIT. The magnetic trap that has been built in Turku will have approximately 100 times the effective volume of the MIT trap, and as such, we will be able to work with much larger ensembles of atoms and will be able to probe many phenomena which were out of reach in the previous experiments by MIT. Working with low density gas out of thermal equilibrium, we will select ensembles of atoms with smallest velocities, which will provide optimal conditions for spectroscopy of H↓ gas.

We shall be performing several measurements for which having proper bolometers is essential for our experiments' success. These planned measurements will be briefly outlined below according to the project's research plan, to give proper context for the purpose of our bolometer chips.

In our spectroscopical studies of H↓ , we wish to detect the two-photon 1S-2S transition in H↓ with resolution approaching natural linewidth (NLW $\sim$ 1.3 Hz). Natural linewidth has never been observed for atomic hydrogen, and its measurement would help provide data on the lifetime of the metastable 2S state, and help understand its relaxation mechanisms. Previously major limitations in reaching this NLW resolution were effects of 2nd order Doppler broadening and short interaction time of atoms with light. For our trap, we can have atoms moving at velocities of several centimeters per second, for which these effects should be reduced by at least two orders of magnitude. A third process that needs to be accounted for is the photoionization of the atoms with absorption of a third photon. This process occurs at high light power, and has not been properly studied. As it may affect the

natural lineshape, it should be studied as a part of this experiment.

Second, we shall measure the 1S-2S resonance frequency shifts caused by interatomic interactions. This measurement will be done for high density gas in the quantum degenerate regime for both normal gas and BEC. In this area there were previously discrepancies between experimental results by the MIT group and theory, which shall be verified and investigated.

The third planned measurement is the optical spectroscopy of hydrogen atoms near superfluid helium surface. We shall again choose the slowest atoms at velocities of several centimeters per second, and deliver them onto the superfluid helium surface. At such low energies, the hydrogen atoms will form gravitational quantum states above the surface, separated by distance of the order of 1-10 μm. These quantum states have a separation of the order of several hundred Hz, which we should be able to clearly resolve with the estimated resolution of our optical spectroscopy. In addition to the gravitational states, there will also be an adsorbed state delocalized at around 5 Å above the surface. An interesting question is whether it will be possible to observe tunneling of hydrogen atoms from the lowest gravitational quantum state to this adsorbed state. With this experimental setup we can also measure the adsorption probability of hydrogen atoms onto the helium surface at ultra-low energies, since the existing data [3, 4] on this do not agree with each other.

Lastly, we shall perform Ramsey spectroscopy with atomic clouds. We can generate a fairly large cloud of ultra-slow atoms, for which we will implement the Ramsey technique of separated oscillatory fields for accurate determination of optical 1S-2S and hyperfine transition frequencies. Typically Ramsey experiments are performed with beams of atoms subsequently passing two excitation regions, or in a fountain of atoms. We will use the technique for a very large ensemble of atoms, with good control of the velocity of the cloud as a whole, providing a very good signal-to-noise ratio (SNR). For both types of spectroscopy, the Ramsey method allows us to

eliminate many systematic uncertainties, and is therefore the most accurate method for accurate determination of transition frequencies.

For each of these experiments we shall be using a laser to provide the excitations, and are planning on using the bolometers as detectors both for simply diagnostics of our hydrogen gas and the laser system and its functionality, and the spectroscopical measurements themselves. Therefore it is of utmost importance that we design and prepare proper bolometers, as they will be essential in ensuring the quality of our system and measurement results. Since we are aiming on the detection of single atomic excitations, equivalent in energy to a single UV quantum, we must attempt to build highly accurate bolometers with a high resistivity dependence on temperature and a low thermal capacity, so we can notice even extremely small temperature changes. In addition, as we are working with a magnetic trap, and will therefore of course have magnetic fields at the location of the bolometer, we should aim for bolometers that have either none at all or an extremely low dependence of resistivity on magnetic field. We will not be working at high fields, as per the specifications of the trap we would not expect to have fields in excess of 1 T, but any potential error source should still be eliminated if possible.

2.2 Detection of atomic hydrogen

While hydrogen as the most simple atom is of course a cornerstone of fundamental physics for testing theories in very simple systems, actually detecting atomic hydrogen can be quite difficult, since hydrogen atoms are of course extremely small in both size and mass, electrically neutral, and their interatomic interactions are very weak.

Detection methods for atomic hydrogen can be roughly categorized into two categories: destructive and non-destructive methods, depending simply on whether the method of detection will destroy the sample. As an example of a destructive

measurement, Silvera and Walraven suspended a carbon bolometer chip covered by a ^{4}He layer in a sample cell filled with atomic hydrogen [5, pp. 196-197]. They then set a current through the bolometer to boil off the ^{4}He layer, which allowed the H$\downarrow$ atoms to condense on the bolometer surface and recombine at a rate defined by the time constant $\tau \simeq \frac{4V}{\overline{v}A}$, where V is the sample cell volume, $\overline{v}$ is the average atomic velocity, and A is the bolometer surface area. This is quite a common technique, widely used in a multitude of experiments (e.g. [6, 7]).

This method actually gives us two basic modes of operation for our bolometer, one where it's covered by the helium film and very few recombination events take place, and one where the helium film has been evaporated, triggering a rapid recombination of the entire hydrogen sample. Technically speaking, we can also define a third mode of operation where we overheat the bolometer, but not enough to evaporate the helium film. In this mode the slightly heated bolometer will interact with the hydrogen gas, which will slightly cool it. This can be used as a non-destructive method of hydrogen detection, as it's quite easy to see the difference when the bolometer is being cooled by the hydrogen gas as opposed to vacuum, where practically the only source of cooling would be along the wires the bolometer is connected to.

With a sensitive enough bolometer it is possible to measure quite accurately the number of recombination events, since the recombination energy is known. This method can be used to measure the number of H$\downarrow$ atoms that was in the sample cell, albeit the sample is of course completely destroyed via the recombination. For our experiments, this is the first diagnostic method we will be using to see whether the H$\downarrow$ samples we create are indeed properly trapped, and how large samples and densities we can create.

Two good examples of detection via non-destructive methods would be detection via optical spectroscopy and magnetic resonance. The difficulty with optical

spectroscopy of hydrogen is the very short wave-lengths needed for transitioning between the available electron states. For example the Lyman-α transition from 1S to 2P is at 121.567 nm, which is situated in the vacuum ultraviolet range, requiring quite expensive and complex laser sources and optics to be set up to allow such measurements. Direct Lyman-α spectroscopy for hydrogen has of course been performed [8], but another often used method is using two-photon spectroscopy, where two photons rather than one are used for excitation. This allows for using lower energies for single photons than with single photon excitations [9].

Since hydrogen has electron and nuclear spins, both ESR [10] and NMR [11] methods are available for experiments on atomic hydrogen. While these are not used as a direct measurement methods, they are immensely useful for the manipulation of atomic hydrogen in the form of RF induced cooling. Hydrogen in it's ground state has four hyperfine states (see fig. 2), two of which (a and b) are high field seeking states and the other two (c and d) are low-field seekers. At low magnetic fields only the doubly polarized d state has a positive energy slope, meaning that with low fields, it is the only state which is trapped by a magnetic field minimum. With RF cooling, we can use ESR and NMR to change the trapped atoms out of the d state, which causes them to be ejected from the trap. The basic idea of RF cooling is that by selectively flipping the states of the higher energy atoms in the trap, we can gradually remove all of the high energy atoms, leaving only the lowest energy (and therefore temperature) atoms [12]. This technique is essential for reaching BEC in atomic hydrogen.

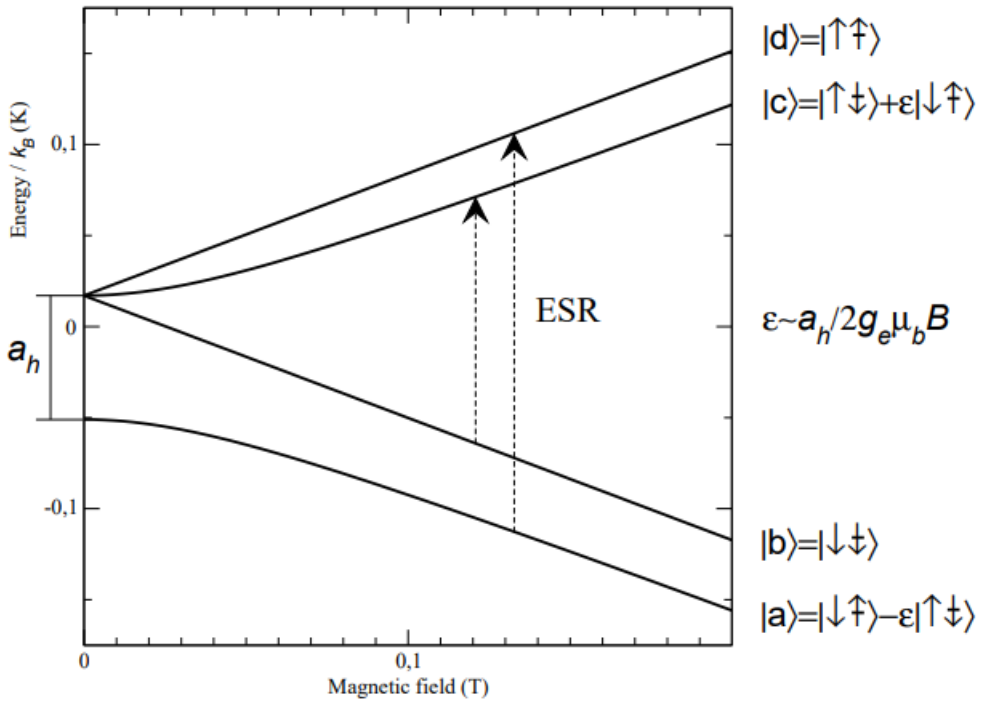

Figure 2: Hyperfine splitting of hydrogen energy states in magnetic field [13]

2.3 Variable range hopping

Since we are working with doped Si bolometers, it's quite important to understand the main processes dictating the behaviour of a doped semiconductor at cold temperatures. For impure semiconductors, Variable Range Hopping (VRH) is the main theory describing their low temperature conductive properties. VRH was initially formalised by N.F. Mott [14, 15] as a theory to describe amorphous semiconductors. In this text we will give a brief, qualitative introduction of the processes will be given on VRH theory, and relevant formulae used for depicting the low-temperature behaviour of doped Si. For the more mathematically inclined and interested readers, a more complete description may be found in literature, for example: [15–17].

The basic idea behind VRH is that charge carriers in the bulk may be thermally excited to higher energy levels, which allows for them to hop to a lower energy state at a different site in the lattice. The conductivity is essentially dependent on the

density of impurities in the lattice, as it is mostly the impurities that generate the free states for the carriers to hop to. The available excitation range, and as a result the hopping range, is of course given by a statistical distribution, which itself is a function of temperature.

On the other hand, the larger picture of macroscopic conductivity (and therefore resistivity) can be understood as a kind of percolation system, where carriers can hop between lattice sites within a temperature-dependent hopping range, forming paths through the entire lattice for charge to flow through. As temperature changes, some of these paths may close and others open. Since the impurities and therefore free states to hop to are essentially randomly distributed in the lattice, it's a very good example of a classic site percolation system. Percolation theory can be used to accurately model and study the process [18], which will indeed lead to the same results as Mott's original formulation.

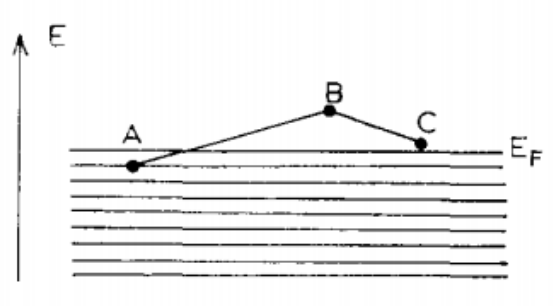

Figure 3: Illustration of the hopping process [15]

Now that an intuitive idea of how VRH functions has been established, mathematically speaking in VRH the general form of resistivity can be presented as:

$$\rho = \rho_0 e^{(T_0/T)^\beta} \tag{1}$$

In Mott's original model we have $\beta = \frac{1}{4}$ [14], but it has afterwards been shown that especially at low temperatures, a model using $\beta = \frac{1}{2}$ is more accurate [19], especially at low temperatures. These regimes where β is $\frac{1}{4}$ and $\frac{1}{2}$ are called the

Mott and Efros-Shlovskii regimes, respectively, and the transition between the two has also been investigated, and a universal (albeit much more complex) form has been found [20].

An example of experimental results showing that this theory properly describes conductivity in semiconductors can for example be found in Mott's paper [15], where measurements of vanadium oxide VO_x are presented. They noted that with $x < 1$, VO_x seems to have metallic behaviour, while for $x > 1$ semiconductor-like behaviour of the resistance as described by eq. (1) could be observed. As can clearly be seen from fig. 4, $VOx > 1$ is properly described by eq. (1) using $\beta = \frac{1}{4}$ in the measured temperature range $T^{-1/4} \in [0.23, 0.7]$, which is roughly equivalent to a measurement range from room temperature at around 300 K to liquid helium temperature at 4.2 K. It's worth noting that at this high of a temperature we wouldn't yet expect to see a transition to the Efros-Shlovskii $\beta = \frac{1}{2}$ dependence.

For our purposes, we can simply fit a piece-wise function for our bolometer calibration if we see that a simple fit with a constant β value will not work, so the universal form is not strictly necessary for our purpose. Whether we need to account for this change in regime will be apparent from our calibration curves when we attempt calibration at sub-kelvin temperatures.

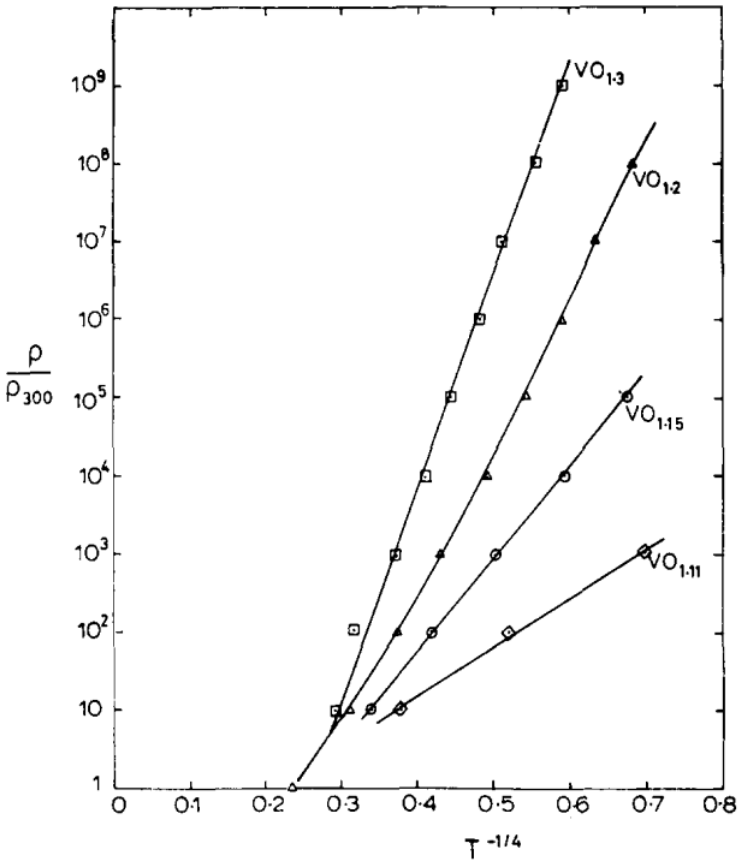

Figure 4: Measured resistivity of VO_x as function of $T^{-1/4}$ [15], showing temperature behaviour $\ln \rho \propto T^{-1/4}$, as predicted by Mott.

2.4 Motivation for choosing silicon bolometers

There are already ready methods to create bolometers, whether from carbon [21], Aquadag [22], silicon [23] or a number of other materials. In a sense, practically any material with a high $\mathrm{d}R/\mathrm{d}T$ is suitable as a material for bolometers. With already-established methods and materials to build bolometers, why are we so interested in going through the effort of finding a suitable material, design and building method for a new bolometer, rather than simply relying on the results of previous efforts?

Truth is that the previous methods are either quite difficult or expensive, or the end result is sub-optimal in one way or another. While previous experiments showed that silicon bolometers can be very accurate and can be well characterised

with respect to their doping concentrations [23], the work and resources put into their work are far more than most smaller research teams would have available. Therefore we wish to find out whether we can use cheap, commercially made silicon wafers and easily accessible, affordable tools and methods to build bolometers of comparable levels of accuracy and precision to the ones built by Adami et al [23]. Should we find it possible to use simple commercial wafers for building well characterized, stable and consistent bolometers, this could enable researchers to relatively cheaply design and produce high quality bolometers for different temperature ranges.

We will now briefly discuss different types of bolometers, comparing their specifications, advantages and disadvantages to shed further light on the reason we chose to undertake this research, and why silicon specifically was chosen.

2.4.1 Aquadag bolometers

In the past, Aquadag bolometers were widely used for experiments with atomic hydrogen [22, 24], in a similar manner to our currently planned experiments. Aquadag as a material is a water-based colloidal graphite coating, where the graphite particles are approximately 1 μm in diameter. These bolometers have the advantage of being relatively easy to make and have a very steep resistivity slope at low temperatures (see figs. 21 and 23 in section section 3.5), but they have the distinct disadvantage of being highly inconsistent and unstable.

Likely the greatest upside of using Aquadag bolometers is the extremely simple, albeit tedious construction process. Aquadag bolometers are made simply by painting a substrate surface with Aquadag, letting it dry, and repeating until a thin (2-20 μm) layer has been formed. The room-temperature resistivity of the layer was then measured to see whether it indicates proper low-temperature behaviour. After this, the bolometer needs to be cooled to below 1 K in order to verify that its resistance falls into the range of 10-100 kΩ in the desired temperature range of 100-200 mK.

Often this is not the case, and the device must be discarded and the process begun again from the beginning.

The surface formed is essentially layered carbon flakes sticking to each other. This for the most parts explains the inconsistency of the properties of these bolometers, as well as their mechanical instability. The fact that the conductive carbon layer is comprised of flakes means the layer is very porous, and that the surface area connecting each of the flakes to the next one is quite small. The porousness means that it's difficult to predict the exact resistance simply by thickness of the layer, which leads to the previously mentioned tedious process of having to continuously measure the resistivity of the bolometer and hoping that proper low-temperature behaviour follows.

Another downside of a flaky structure is that even small vibrations may easily damage the structure, changing the bolometer's properties enough to require recalibration. This was to the extent that if someone accidentally bumped the cryostat, this may have ruined the calibration. The small contact area also leads to poor thermal conductivity, and the bolometers had quite a high specific heat.

For carbon resistors, it turns out they actually obey the same eq. (1) as used in VRH theory to describe low-temperature resistivity [24]. We can indeed see from calibrations done by Hydrogen Research Group (see fig. 21 in section section 3.5), that the temperature dependence seems to be very similar for Aquadag bolometers as for the germanium chips, which are very classical semiconductor materials covered by VRH theory.

Additionally, it was discovered that Aquadag bolometers have a noticeable negative magnetoresistivity (see fig. 5), meaning the resistivity is also dependent on magnetic field, which would be problematic for our experiment, where the magnetoresistivity should be negligible at least up to 1 T, which is the maximum field for our trap.

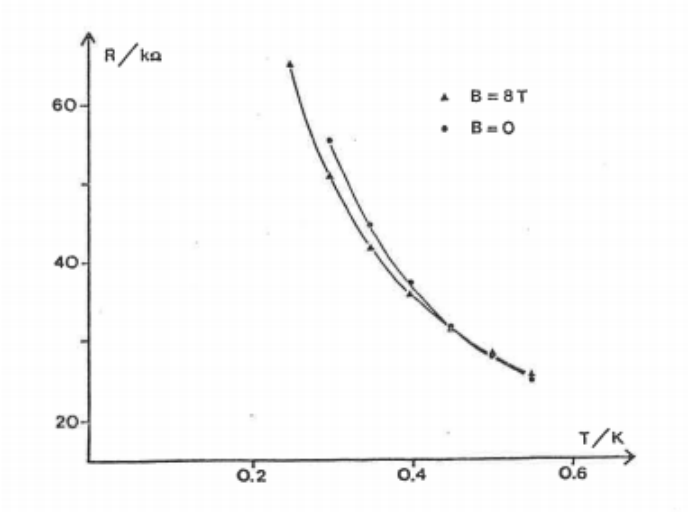

Figure 5: Aquadag resistance with and without 8 T magnetic field [24]

2.4.2 Transition-edge sensors

Transition-edge sensors are based on the simple fact that superconducting materials have a very steep change of resistivity from a finite value to zero at their material-specific transition temperature (see fig. 6) [25]. Transition-edge sensors are extremely sensitive in their temperature range, albeit as a result of the rapid transition their operational range is also quite limited. Transition-edge sensors have a very good time resolution, which is part of the reason for their relative popularity in the field of particle physics, where time resolution can be of great importance.

Transition-edge sensors are a well developed invention, and are extremely accurate in their operational range. They have been used in a multitude of projects ranging from the LHC at Cern [26] to measurements of the cosmic microwave background [27]. However, for our project they are not an optimal choice of sensor for several reasons. First, the operational range of a transition edge sensor is simply too narrow for our experiments, as any large amount of recombinations would simply overheat the sensor out of operational range. Also, it's well known that an external magnetic field will cause broadening of the superconductor transition and will shift the transition temperature, meaning transition-edge sensors cannot be used

in the presence of a magnetic field, rendering them unusable in our magnetic trap experiments. SQUID amplifiers usually paired with transition-edge sensors are also inoperable in magnetic field. Finally, due to their narrow operational range, we cannot utilize multiple measurement modes (see section 2.2) unlike with sensors not based on superconductors.

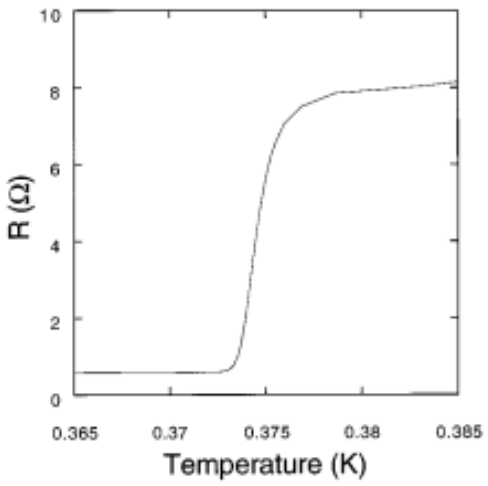

Figure 6: Measured resistance curve around transition temperature for a titanium film transition-edge sensor [28]

2.4.3 Ruthenium oxide chips

As was said before, basically any material with a strong dependence of resistivity on temperature at our preferred temperature range can function as a bolometer. A good comparison readily available at the laboratory were commercial ruthenium oxide chips, which have been calibrated for low temperatures. There's nothing all that special about these chips, they have often been used as temperature sensors in experiments by the Hydrogen Group over a long time, and have been deemed quite stable, without need to recalibrate practically ever.

Ruthenium oxide resistors are essentially thick RuO_2 films on top of a substrate, and can be purchased from different manufacturers around the world as ready-made and calibrated chips. In addition to purchasing ready chips, there is the possibility of

using commercial RuO_2 paste, which contains small RuO2 grains, to manufacture our own thick film resistors. This process is described for example in [29], and consists of first depositing the paste onto an alumina (Al_2O_3) substrate, then drying it at 150 °C and finally heating it to 850 °C for 10 minutes. While manufacturing these films by hand will likely lead to less consistency, it does allow for free choice of geometry and size, unlike with commercial ready-made chips.

The conductivity mechanism in RuO_2 is not well known. There have been attempts to describe its low-temperature conductive properties through both VRH theory and theories specifically generated for thick film resistors, but no single theory has been found that would properly describe the low temperature resistivity of ruthenium oxide [29, 30], despite VRH theory giving a decent estimation except at very low temperatures, as an example we can see from fig. 7 that down to approximately 100 mK the resistor follows Mott regime VRH behaviour quite nicely, but deviates at lower temperatures.

While ruthenium oxide has been found to have a relatively low magnetoresistance above 100 mK, when going below 100 mK the magnetoresistivity suddenly increases rapidly [31]. This is, once again, enough reason for us to decide against using RuO resistors as bolometers for our experiment, despite their apparent ease of use and low price.

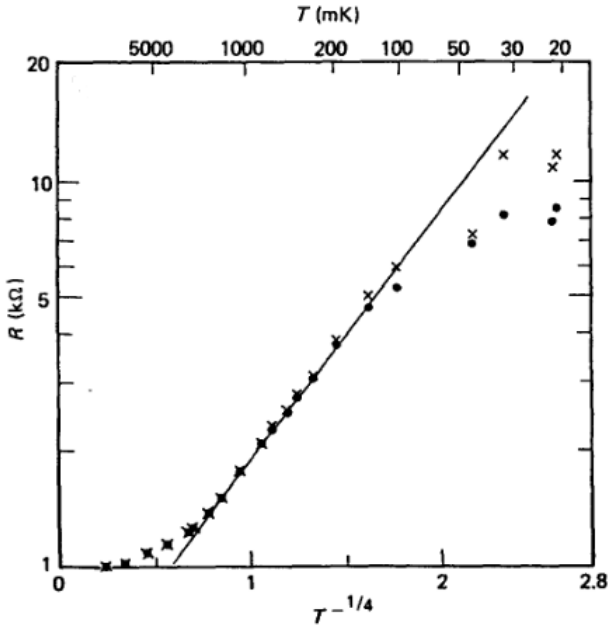

Figure 7: $R(T^{-1/4})$ for two Dale Electronics 1 kΩ resistors, • and x denoting the two sets of measurements. [32]

The main advantage for this type of chips is their extremely low price and the fact that they can be easily bought in bulk with a ready calibration, or custom-made at the laboratory with paste if need be. However, manufacturing such chips at the laboratory is no longer as easy due to requiring an alumina substrate and a high-temperature oven. Additionally, it turns out we can build far more sensitive bolometers from semiconductor materials (see section 3.5).

2.4.4 Semiconductor based bolometers

Doped silicon bolometers have been used quite widely, and there's ample research on using them as both thermometers and bolometers [23, 33, 34]. The process defining conduction in semiconductors at low temperatures is of course the Variable Hopping Range theory, as per eq. (1). Here we shall present three materials that have been proven to be good candidates for low temperature bolometers: Silicon, germanium and gallium arsenide (GaAs).

Gallium Arsenide has been shown to have a rather nice VRH behaviour at low

temperatures [35], but it is ill suited for our purposes due to its magnetoresistive properties [36].

Germanium can be used as an excellent thermometer at low temperatures. Vadim F. Mitim and his company "Microsensor" (Kiev, Ukraine) have produced a lot of germanium chips meant for low temperature applications. Specifically, they manufactured resistance thermometers based on Ge films deposited on a GaAs substrate via evaporation. This leads to an interesting Ge-GaAs heterostructure, where the Ga and As atoms can diffuse from the substrate to the Ge film, changing its electrical properties [37]. By controlling the parameters of the deposition process and via different chemical and physical treatments they were able to control the process and determine the electrical properties of the Ge films. Within the film, Ga atom defects function as acceptors, while As atoms act as donors, leading to both doping and compensation in the Ge film.

These germanium film sensors were relatively reproducible (see fig. 8), and they were quite stable, requiring only slight recalibration over several years (see fig. 9). In addition, the germanium chips actually have a rather nice and steep $\mathrm{d}R/\mathrm{d}T$ at low temperatures, as can be seen from fig. 8. The main downside, once again, is that it has been well documented that germanium also has quite a strong magnetoresistivity effect, rendering it unsuitable for our magnetic trap applications [37, 38].

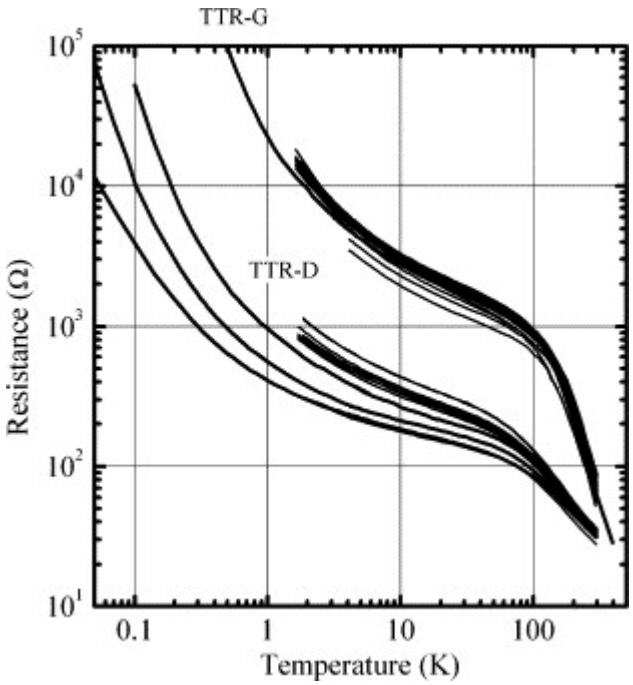

Figure 8: $R(T)$ graphs for two thermometer models (TTR-G and TTR-D) manufactured by Mitin at Microsensor from a single batch of wafers [37].

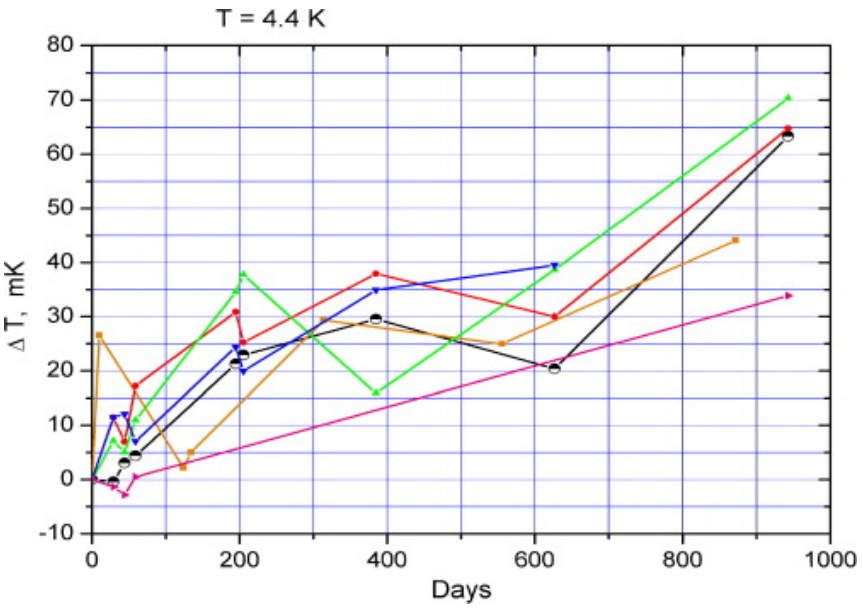

Figure 9: Graph showing the stability of TTR-G germanium thermometers over a 2.6 year time period [37]

Lately silicon bolometers have been gathering more and more interest in the scientific field, with a lot of potential applications in various applications from phonon

detection [39] to infrared detectors [40] and astronomy [23]. Silicon as a material is relatively cheap and methods for its processing are well developed and widespread, so acquisition of silicon is relatively easy and cheap, depending of course on the exact specifications of silicon needed. Additionally, silicon is only very weakly magnetoresistive at low fields [41], albeit as this can be highly dependent on dopants chosen and doping concentration, it should be experimentally verified.

There has been some very nice research by Adami et al [23] into characterization of the VRH behaviour of doped silicon with different doping concentrations. The samples used in their research were phosphorus-doped silicon with boron used as a compensator, likely to fine-tune the resistivity. The process of manufacturing these chips is described in another paper [42]. They used ion implantation for doping the silicon samples, which allows for good control of the doping concentration.

The chips produced by Adami et al [23] were characterised according to their resistance values at 100 mK and their T_0 parameter as defined in eq. (1), which tells us about the proper temperature range for such sensors can be used in, since T_0 defines the temperature dependence. Full table of their characterised chips can be seen in fig. 10. It's worth noting, that as ion implantation was used for doping, as a result the doped conductive layer is quite thin, leading to relatively high total resistances. For our project we are mostly looking at commercially produced wafers where the entire bulk is doped, which allows for lower total resistivity, making measurements easier.

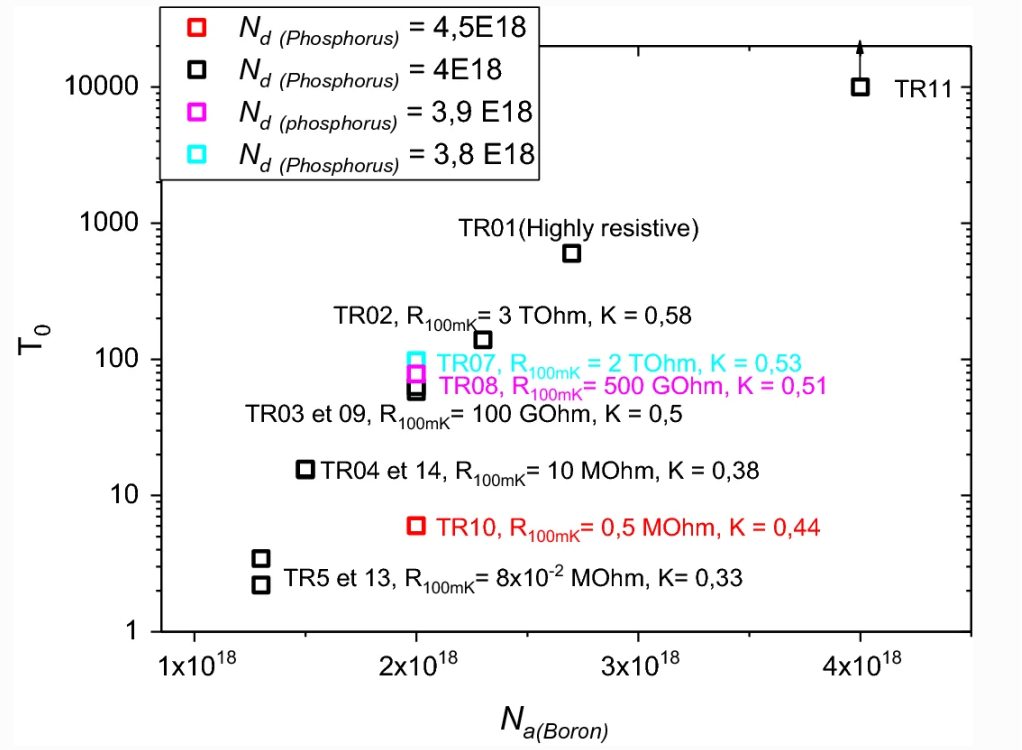

Figure 10: Chips tested by Adami et al. Chips with four different P doping concentrations N_d were tested and their T_0 parameter is shown as function of B compensation concnetration N_a. Resistances of chips at 100 mK are shown in the graph. [23]

Doped semiconductor samples can be manufactured with a variety of methods. Some of the more commonly used ones are the Czochralski method and Floating Zone methods. These two methods shall not be described here in detail except for the fact that due to being processed in vacuum, floating zone method generally produces crystals with fewer impurities [43]. Most doped silicon wafers available commercially will be prepared using one of these two methods. However, another option specifically for silicon would be neutron transmutation, based on the reaction $^{30}\mathrm{Si}(n,\gamma)^{31}\mathrm{Si} \rightarrow^{31} \mathrm{P} + \beta^-$ [44]. Another possibility is ion implantation as used by Adami et al [23, 42], where dopant atoms are directly implanted into the silicon by simply accelerating dopant ions into the target. This method of course cannot be used to dope thick targets, but will instead result in a layer of doped silicon on top of an undoped bulk. After ion implantation, thermal annealing is required to repair

damage caused by the accelerated ions [42].

With neutron transmutation according to the $^{30}\mathrm{Si}(n,\gamma)^{31}\mathrm{Si} \rightarrow^{31} \mathrm{P} + \beta^-$ reaction mentioned previously, one can use non-doped wafers prepared by other methods (e.g. floating zone), and by placing the crystals into a neutron reactor, it is possible to use neutron radiation to introduce phosphorus dopants to the crystal lattice in an extremely homogeneous manner and with a very accurately controllable dosage. This can be seen for example in the fact that with neutron transmutation, it is possible to reach resistivity fluctuations of approximately $\pm 3\%$, with a $\pm 7\%$ resistivity tolerance level, far better than other doping methods [44]. The downsides to this method are of course quite obvious: Due to the secondary reaction $^{31}\mathrm{P}(n,\gamma)^{32}\mathrm{P} \rightarrow^{31} \mathrm{S} + \beta^-$ resulting in radioactivity of the sample with a half-life of approximately two weeks [44], silicon wafers produced in this manner must be allowed to decay to safe limits of activity before use. Additionally, since this method of course requires the use of a special neutron source, the availability of this method is relatively limited.

Silicon was deemed an optimal candidate material for our bolometer chips, because it is relatively cheap, it has been widely studied, and wafers of different doping concentrations are readily available for easy testing. In addition, their magnetoresistivity below 1 T fields is quite low, which is extremely important for our measurement accuracy. Bolometers made of silicon can also be expected to be far more stable and less prone to damage than for example the Aquadag bolometers used in previous experiments. Additionally, the work done by Adami et al [23] gives an excellent starting point to allow us to narrow down the resistivity and doping concentration range we should test for proper VRH behaviour.

3 Experimental work

3.1 Background

As there is no perfect theory to accurately predict the temperature at which variable range hopping becomes the dominant process determining resistivity, we began looking for suitable materials from commercial doped silicon manufacturers, by simply buying wafers of various doping concentrations and experimentally measuring their resistivity behaviour at low temperature. Manufacturers in general do not give the exact doping concentrations for their wafers, but rather characterize them by their room-temperature resistivities. Most manufacturers use Boron or some other acceptor dopant to fine-tune the resistivities of their wafers. This is slightly problematic, since as we know from the work of Adami et al [23], the VRH behaviour is dependent on both the donor and acceptor dopant densities, thus making an accurate prediction of the low-temperature behaviour from only the room-temperature resistivity is quite difficult. However, room-temperature resistivity is still a decent indicator of at least the magnitude of doping, and serves as an approximate indicator for classifying low-temperature behaviour.

As we are mainly interested in bolometers operating at temperatures below 1 K, we must finally check the samples in a dilution refrigerator to properly test whether a sample is good for building bolometers. However, as testing samples in a dilution refrigerator is quite slow and difficult, we started with measurements at higher temperatures and tried to pinpoint a proper room-temperature resistivity range where we could look for suitable sub-kelvin bolometer materials.

For this purpose, we cut out small rectangular pieces from the acquired commercial silicon wafers, and placed them in a Physical Property Measurement System (PPMS) to measure the resistance of the sample as a function of temperature. While the PPMS can only go down to a temperature of two kelvin, this should be enough

to predict whether the samples would be likely to have a large $\mathrm{d}R/\mathrm{d}T$ in the designated temperature range below one kelvin. Further tests for promising samples were conducted in a dilution refrigerator to measure their behaviour at lower temperatures.

3.2 Sample tests with PPMS

The resistance of our sample is measured via a four-wire DC measurement. The silicon chips were glued onto a PPMS insert, first using two-sided tape, but due to occasional detaching from the tape during measurement, the samples were later glued to the insert with varnish instead. The four contacts were made via wire bonding, using a 30 micrometer thick aluminium wire (See fig. 11). Current was applied to the sample using a Keithley 2614B source meter, and the voltage was measured using an Agilent 34420A volt meter.

For each set of measured samples we also captured a picture to approximate the geometry of the silicon sample, so we could calculate the geometrical factor to convert measured resistance to resistivity. This measurement was simply done using an image editing program to measure the widths and lengths of the samples in pixels and comparing them to the 13.5 mm $\times$ 11.5 mm sample holder area. It was not necessary to measure the thickness in this way, since the wafer thickness was simply given by the manufacturer.

While inaccurate cleaving of our samples usually results in slightly trapezoid-shaped samples, for this measurement we simply assumed the samples to be roughly rectangular. This is a relatively harmless assumption, as the error is relatively small (See appendix section A for derivation and error estimation). It should also be noted that these PPMS measurements are meant merely for narrowing down our selection of test samples in our search for the proper doping parameters for a sub-kelvin silicon bolometer, so a small measurement error is acceptable. This problem

could of course be solved by using a dicing saw that could cut silicon wafers cleanly, but such a device was not readily available for these measurements.

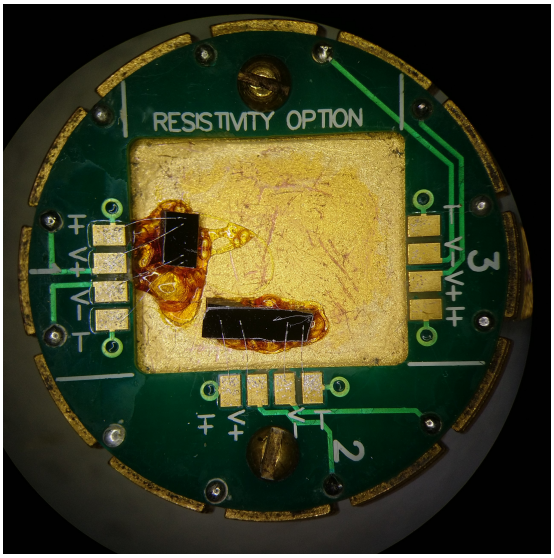

Figure 11: Picture of the PPMS insert with two samples glued on with varnish.

For a rectangular sample, the resistance R assuming homogeneous resistivity ρ can be simply calculated as

$$R = \rho \cdot \frac{L}{A}, \tag{2}$$

where A is the cross-sectional area and L is the length of the measured piece. Length in our case as shown in fig. 11 is determined as the distance between the two inner voltage probes.

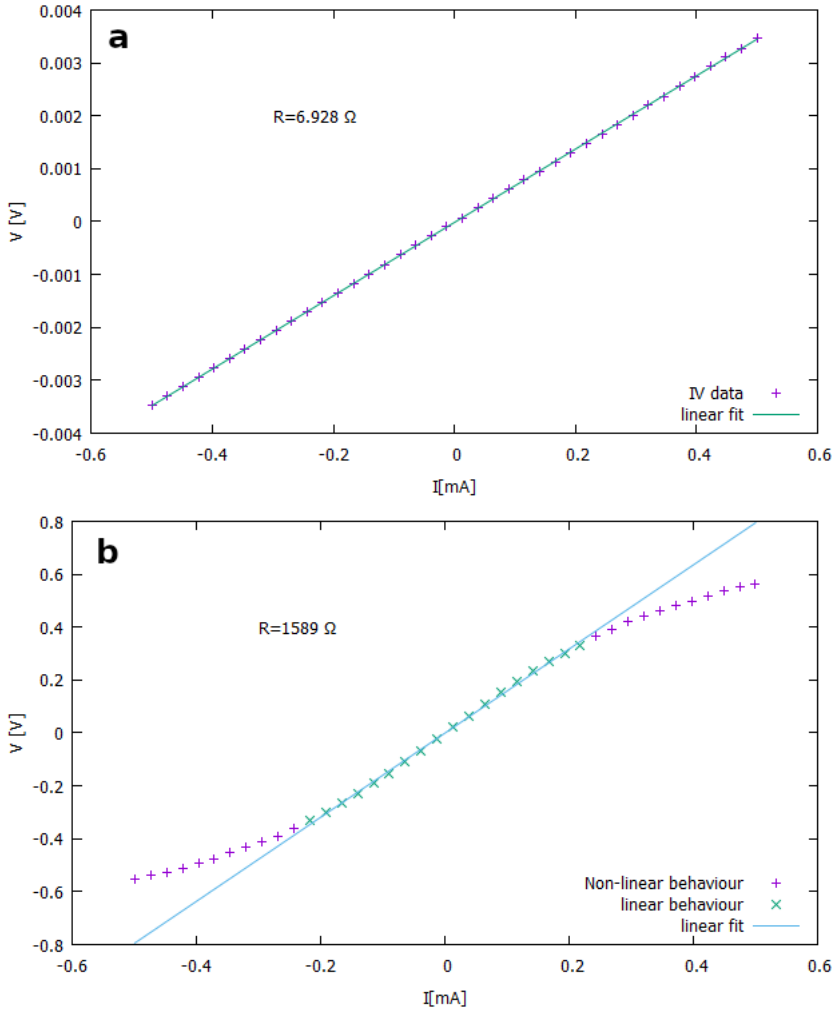

Figure 12: IV-curves showing no anomalous effects (a) and saturation towards high measurement current due to excess heating (b)

For each sample to be measured, the PPMS was given a set of temperatures where the resistance should be measured, and for each of these points the temperature was stabilized, after which the current source and the voltmeter were used to measure a current-voltage (IV) curve of the sample (see fig. 12a). To each IV-curve we can fit a linear function, and from the slope of said function we can extract the resistance of the sample. In addition, we can use the IV-curves to see whether there are any anomalous effects, especially heating induced by too high measurement current, which would show as curving of the IV-curve as the resistivity of the sample would change with heating (see fig. 12b). If the IV-curve indicates overheating, we

decreased the measurement currents and only use the region where the IV-curve is linear for fitting. Once the resistance has been measured, we can use the measured dimensions of the sample to convert resistance to resistivity, which is easier to compare between different samples.

Once the samples are sufficiently tested in the PPMS and we have found the wafers with promising VRH characteristics above 2 kelvin, they will be further tested at sub-kelvin temperatures to measure the exact temperature dependence in the operational range of our experiments.

3.3 Results for temperatures above 1 K

Over the summer of 2020, 13 silicon samples from four different commercial sources were tested with PPMS. Out of the 13 samples, four showed clear VRH behaviour under 10 K. See fig. 13 for the full list with the parameters of the wafers as given by the manufacturer, as well as the experimental values of resistivity at room temperature as measured with the PPMS. While room-temperature resistivity by itself of course isn't very interesting to us, it can be considered a decent indicator of the doping concentration of the sample, which in turn dictates the low-temperature VRH behaviour of the sample and could possibly therefore be used to at least approximately predict the low-temperature behaviour of the sample. It's worth noting that the sample wafers were not ordered at the same time, but rather as our experiments helped us slowly narrow down the proper resistivity range, we bought additional wafers within the range until a proper material could be found.

ID	Manufacture ID	Dopant	R, Ωcm	Exp. R, Ωcm	Thickness, μm	Process	Orient	Polish
3	University Wafer	As	0.001 - 0.005	0.0026	280	-	100	ssp
4	University Wafer	P / B	0.001 - 0.005	0.0048	380	-	100	ssp
5	University Wafer	N / P	0.001 - 0.005	0.0032	500	-	100	ssp
13	Siegert Wafer	N / As	<0.005	0.004	525	CZ	100	ssp
19	**Siegert Wafer**	**N / P**	**0.01 - 0.02**	**0.018(2)**	**385**	**CZ**	**100**	**dsp**
22	Sil'tronix	N / P	0.005 - 0.01	0.016	427 - 437	CZ	100	dsp
23	Sil'tronix	N / P	0.003 - 0.007	0.009	180 - 220	CZ	111	dsp
24	**Sil'tronix**	**N / As**	**0.007 - 0.009**	**0.022**	**500 - 550**	**CZ**	**100**	**ssp**
25	Sil'tronix	N / P	0.005 - 0.01	0.0096	355 - 405	CZ	100	ssp
26	Sil'tronix	N / P	0.009 - 0.01	0.014(2)	500 - 550	CZ	111	dsp
27	Sil'tronix	N / P	0.004 - 0.006	0.0042	361 - 401	CZ	100	dsp
28	**EL-CAT Inc.**	**N / P**	**0.011 - 0.013**	**0.012(5)**	**1000**	**FZ**	**111**	**dsp**
29	**EL-CAT Inc.**	**N / Sb**	**0.011 - 0.016**	**0.0176**	**300**	**CZ**	**111**	**ssp**

Figure 13: List of wafers. Note that R refers to the (room-temperature) resistivity given by the manufacturer, while Exp R refers to experimental data measured with the PPMS. Samples marked in bold showed VRH behaviour. ID column refers to laboratory internal sample identification numbers. In the process column, CZ refers to the Chochralski method and FZ refers to Floating Zone method. Manufacturing companies: University Wafer, Siegert Wafer, Sil'tronix Wafer, EL-CAT Inc.

For each sample the resistance was measured directly by PPMS and via IV-curves between 2 and 300 kelvin at set points, and then using eq. (2) to calculate the resistivities at each point according to the geometry of each sample. It's worth noting, that in multiple cases the measured resistivity differed significantly from the values reported by the manufacturer. Using the measured resistances and sample dimensions we can plot the resistivity of our samples as a function of temperature. The most interesting resistivity plots can be found below.

In the graphs we have plotted the results from PPMS while ramping up and down temperature (Increasing T and Decreasing T, respectively), where resistance was measured at each temperature point using maximum excitation current, and the data calculated from the IV-curves, which should in general be considered the most accurate of the three graphs due to countering some of the heating effects at lower temperatures, as can be seen from fig. 15, for example. At lower temperatures both

of the direct PPMS measurement curves saturate due to heating effects from the high resistivity and the high excitation current. The IV-measurements don't have this problem, as we can remove the high power heating effects from high measurement current by only choosing the low-current points for our resistance fit, where the IV-graph is linear. Of course, the IV sweep must be done slowly enough that the sample can cool down between measured points to prevent the heating effect from affecting the results, but since in our case each sweep took more than 30 seconds, there should've been ample time for the sample to thermalize between points.

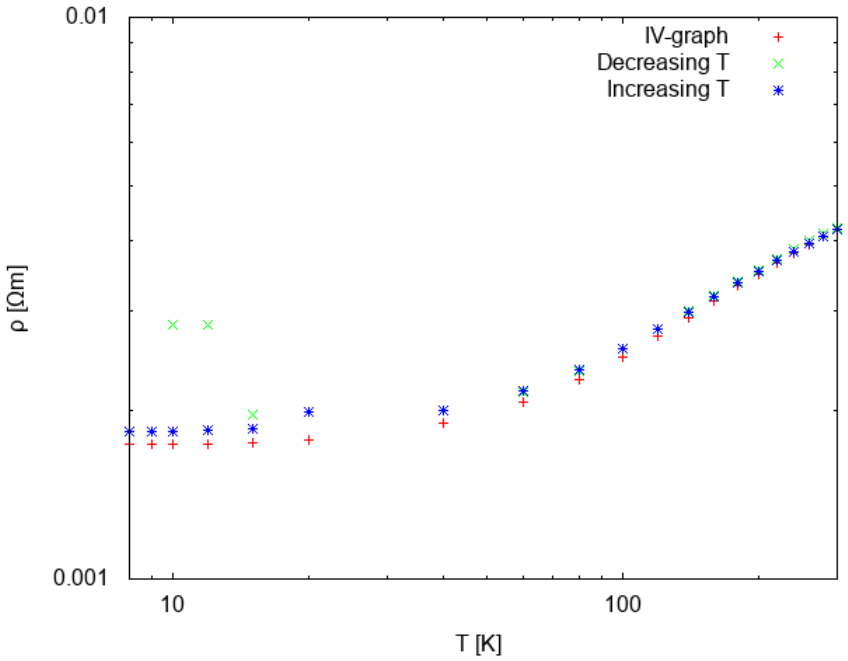

Figure 14: Resistivity curves for sample 27, showing metallic behaviour. Some weird, likely erroneous measurement points were acquired during the cooling process around 10 K.

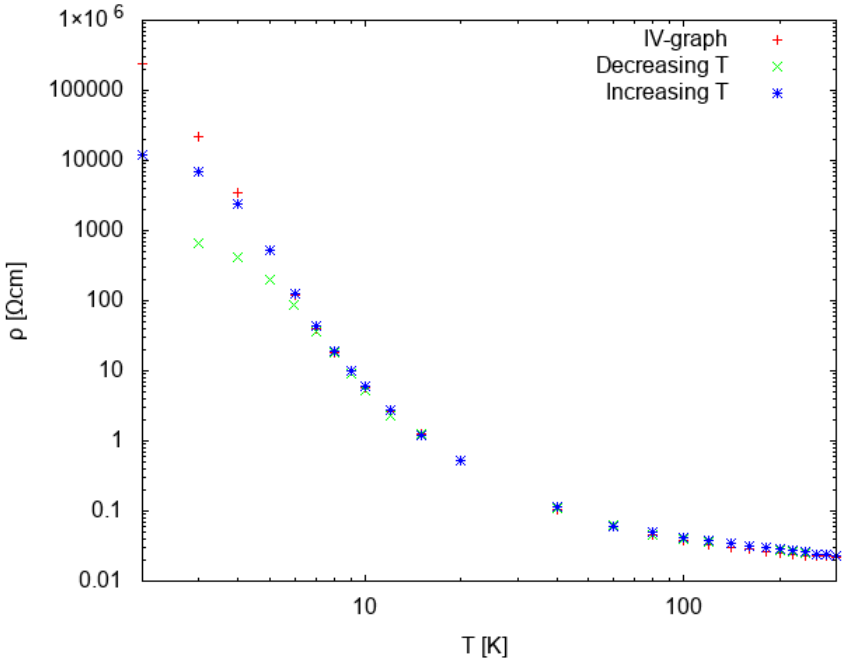

Figure 15: Resistivity curves for sample 24, showing VRH behaviour. At lower temperatures strong overheating can be seen in all but the IV-measurement curve.

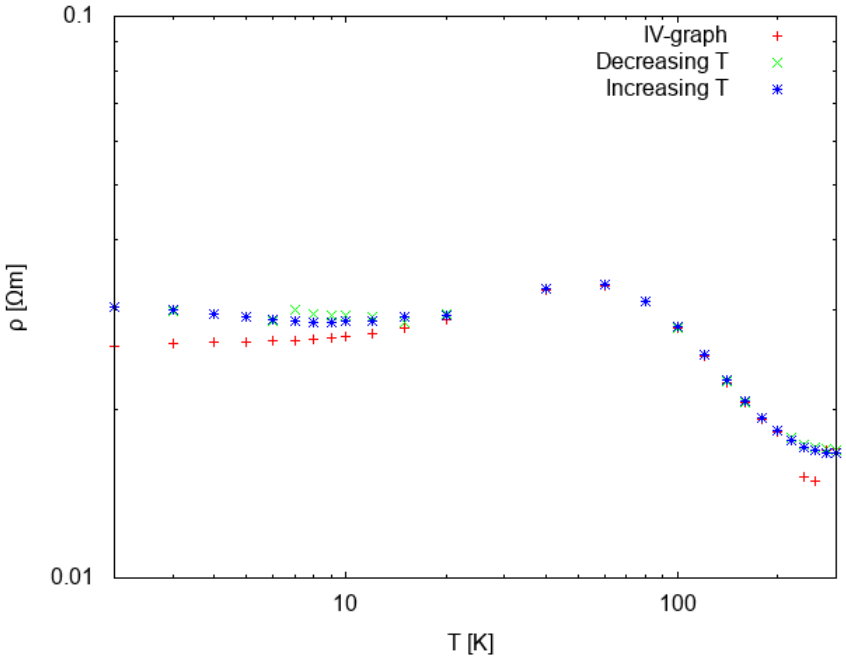

Figure 16: Resistivity curves for sample 22.

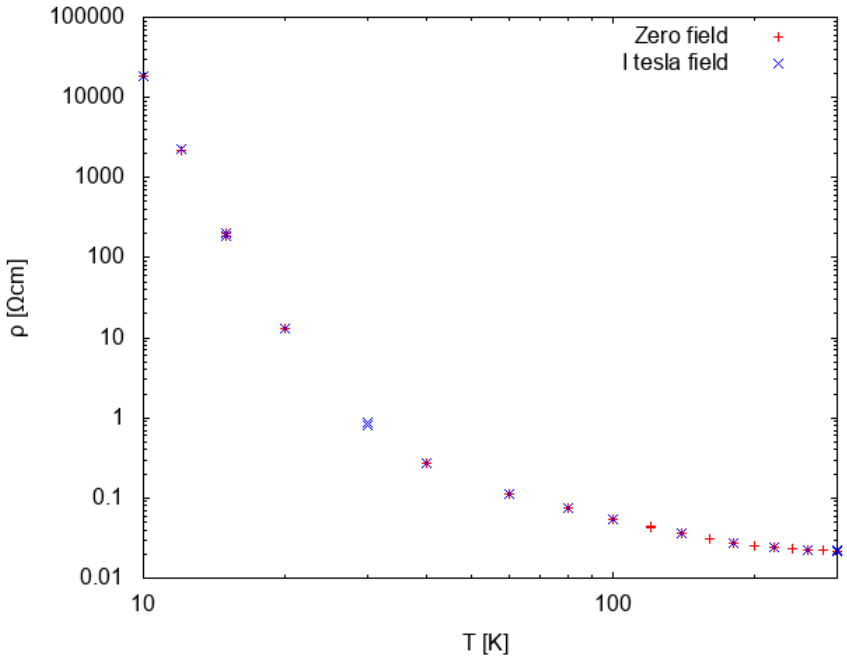

Figure 17: Sample 19 magnetoresistivity measurements, measurement with zero field shown in red, measurement in 1 T field in blue.

In the figs. 14 to 17 above, we have the different general types of behaviour we saw from our samples. In fig. 14 we can see an example of a sample that stays metallic even at lower temperature, with the resistivity continuously decreasing with decreasing temperature. At low temperatures we see some saturation, which can either be some minimum resistivity dictated by the conduction process, or it might be explained by bad contacts. There is no indication of a rise in resistivity as predicted by the VRH theory. This kind of samples can be dismissed from being potential bolometer material, as they are unlikely to show proper VRH behaviour even below 1 kelvin. When taking into consideration the VRH theory, this implies that the dopant concentration for these samples is too high.

On the other hand, figs. 15 and 17 show proper VRH behaviour and show a nice exponential increase in resistivity as the temperature drops. Unfortunately, with these two samples the temperature at which the resistivity starts showing a steep increase is far too high, above 10 K for sample 19 and between 3 and 6

kelvin for sample 24. This would lead to a resistivity of $\rho > 10^6$ Ωcm at sub-kelvin temperatures, which would be very difficult to accurately measure with any realistic excitation levels. The absolute maximum resistance for a chip at our experiment temperature should be at around a megaohm, much higher resistances would make measurement very difficult. Therefore we need a sample where the VRH behaviour starts at a lower temperature. When taking into consideration VRH theory, this implies that the dopant concentration for these samples is just slightly too low.

In addition to the previously discussed samples, samples 28 and 29 showed VRH-like behaviour, and although for sample 29 the resistivity once again began increasing at too high a temperature, sample 28 only began increasing its resistivity at temperatures below 10 K, and even at 2 K its resistivity was still fairly low, indicating the possibility of having the correct resistivity range below 1 K (see fig. 18). Sample 28 will be discussed further in sections sections 3.4 and 3.5, as it showed the most promising behaviour for our practical applications of all the samples.

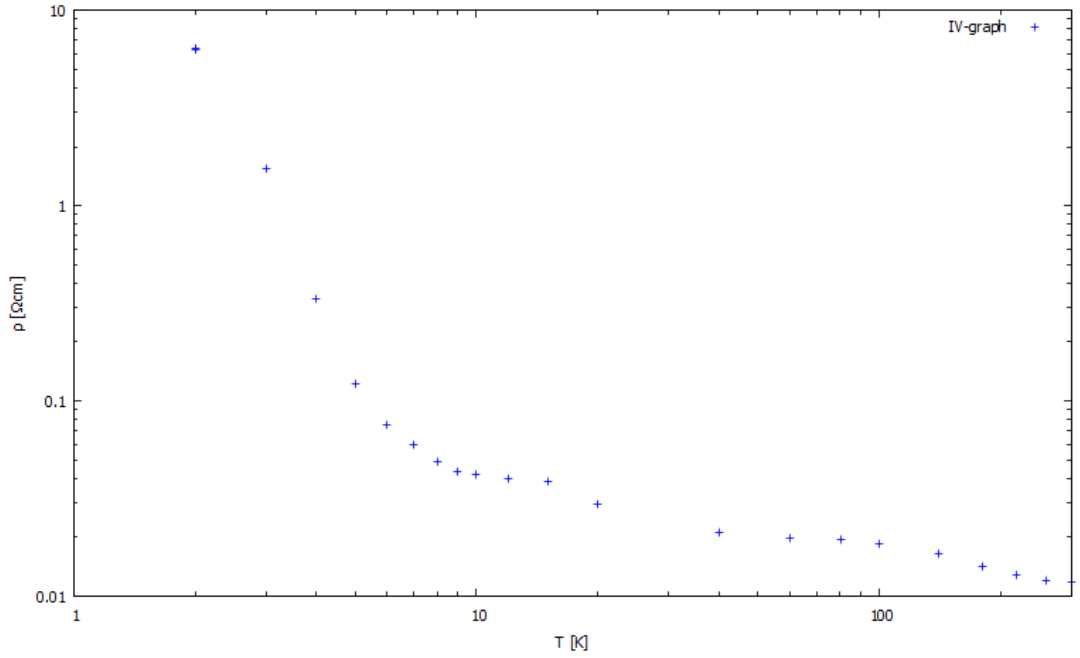

Figure 18: PPMS results for sample 28

As a special case we can look at fig. 16, where we had a strange increase in resistivity around 100 K, followed by a slow decline as the temperature dropped further. This behaviour was not seen in any other samples, and it is difficult to accurately judge the reason behind this effect, but one possibility is that this sample is just barely between metallic and VRH behaviour. Despite the slow decline down to two kelvin, it might be possible for the resistance to rise sharply below 1 kelvin, so it should be one of the samples tested in a dilution refrigerator. Whether or not the sample is a good bolometer, it might provide interesting data.

Since we have both samples with too high and too low dopant concentrations, we can guess that the correct doping concentration should be somewhere in between. As we can assume the dopant concentration is proportional to the room temperature resistivity, we can guess that for the proper doping concentration, our room temperature resistivity should be slightly over 0.01 Ωcm, as per fig. 13. As was already said, since wafer manufacturers often add acceptor dopants to fine-tune the resistivity of their wafers and do not disclose the accurate dopant densities, we cannot accurately find an exact resistivity limit as the acceptor atoms make the situation slightly more complicated. It can indeed be seen from our list of samples (fig. 13) that resistivity alone is not a sufficient indicator of low-temperature behaviour, since although most samples where the room-temperature resistivity was above 0.01 Ωcm showed VRH behaviour, samples 22 and 26 did not, despite being well within the range.

Two factors we thought might have an effect on the resistivity were crystal orientation and magnetic field. Tests revealed that magnetic field had no visible effect on the resistivity curve, as shown by fig. 17. As for crystal orientation, tests we've tried to run have thus far been inconclusive, as we have seen differences in the low-temperature behaviour of samples taken from the same wafer, but said differences could not be reliably pinned on crystal orientation rather than measurement errors. Further tests on this issue should be conducted to clarify.

3.4 Sample tests below 1 K

After the PPMS measurements, samples 22 and 28 were chosen as proper for measurement in a dilution refrigerator. For dilution refrigerator a special sample holder was constructed from standard printed circuit board (see fig. 19a), to which the silicon samples could be attached by pressing them to the sample holder with small copper pins (see fig. 19b). Both the sample holder and the pins were insulated using kapton tape, so as to not form any extra electric contacts to the silicon samples. We used four-wire measurement just like with PPMS, and the sample holder had pads we could wire bond contacts to the sample from (see figs. 19a and 19b). IV curves were measured with a Keithley 2410 sourcemeter, and sample resistance was extracted from a linear fit to these IV curves, just like with PPMS measurements.

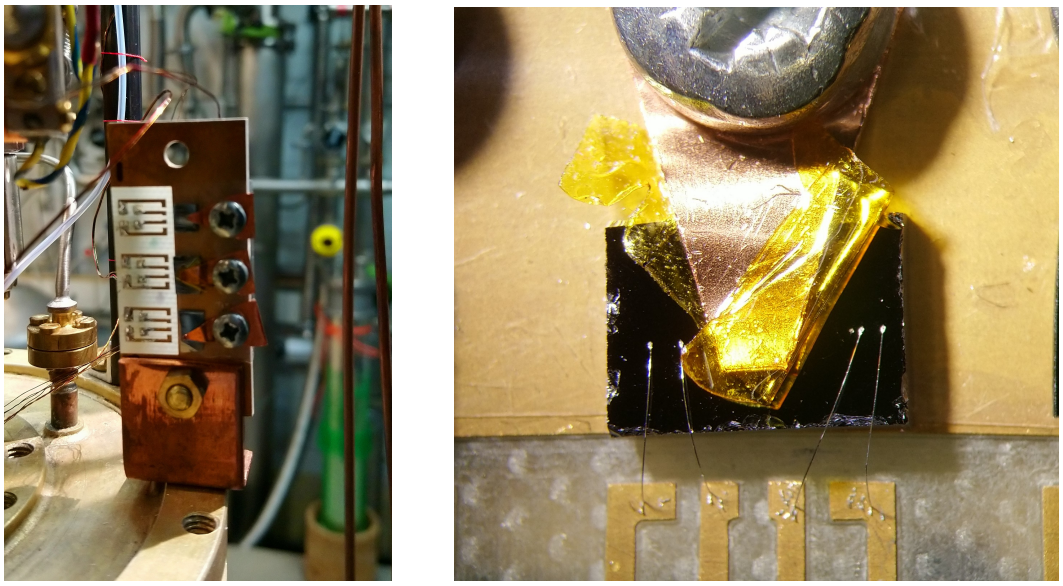

(a) **(b)**

Figure 19: Sample holder in the dilution refrigerator (a) and attached silicon sample (b)

Unfortunately due to technical difficulties, only data for sample 28 could be properly measured. The probable reason for these technical difficulties were bad contacts to the sample. Fortunately though, sample 28 (fig. 20) shows excellent

behaviour, with a very large slope below 1 kelvin temperatures. There were some excess heating effects which caused saturation of the resistance curve at lower temperatures, but the measurement was enough to establish that the sample 28 is an excellent candidate for building sub-kelvin bolometer chips, which will likely be very sensitive in our preferred range. The excess heating is due to self-heating of the samples at low temperatures. The reason for this self-heating can vary, as it can be caused current loops, mains pick-up, leakage of RF-radiation via cryostat wiring or radiative heating. This self-heating is independent of the excitation used to measure the sample, and therefore we can verify that this effect is due to self-heating by lowering the excitation power, and seeing that it has no effect on the saturation of the curve. The most likely reason for the self-heating detected in our experiment is RF pick-up through the wiring of the cryostat, as the cryostat used has a lot of old, improperly done wiring.

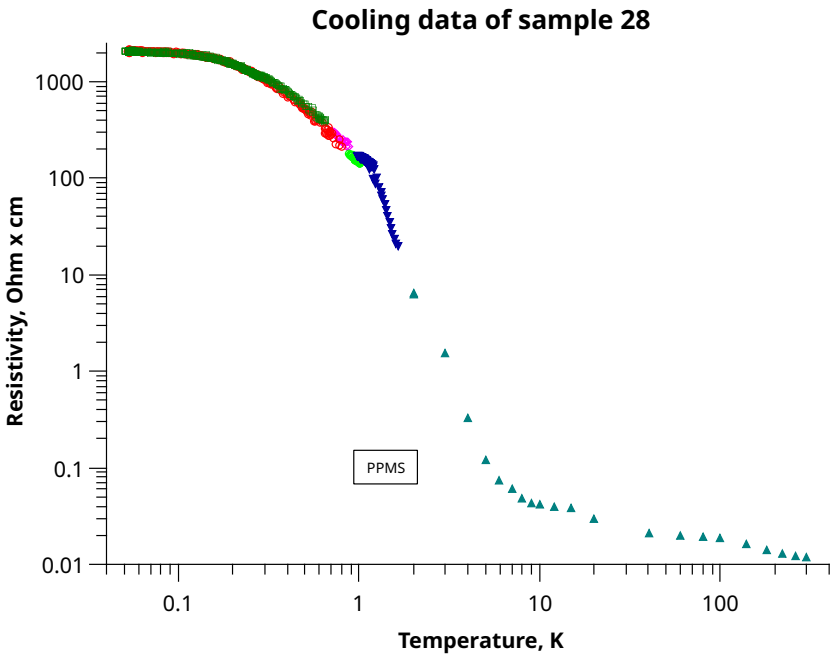

Figure 20: Resistivity of sample 28 in dilution fridge. Different colours refer to separate measurement sets, with teal triangles going to high temperatures being PPMS data.

One surprising feature of the resistance curve was the sudden bend at around 1

kelvin, which is clearly visible on the graph and was repeatable over several different measurements. Reason for this behaviour is unknown, since albeit we could at some temperature see the shift from the Mott VRH regime to the Efros-Shlivskii regime, this should be marked by an increase in the steepness of the slope, rather than the decrease we clearly see on the graph. One explanation could be some error in the measurement system that somehow messed up the dilution refrigerator calibration below 1 kelvin, albeit thus far no such error has been found. This kink in the behaviour of this sample should be investigated further once the excess heating problem has been resolved.

3.5 Sensitivity comparison

To quantitatively inspect the quality of potential silicon bolometer, we will compare the sensitivity of our silicon sample 28 to previously used thermometers. In order to do this, we will plot the logarithmic derivatives $\frac{\mathrm{d}R/\mathrm{d}T}{R}$ (or $\frac{\mathrm{d}\rho/\mathrm{d}T}{\rho}$) of the sample 28, a high quality Aquadag bolometer previously used for experiments, and two thermometer chips, a doped germanium chip produced by Vadim Mitin at Microsensor and a RIVAC RuO_2 chip, both calibrated previously by the Hydrogen Research Group. The logarithmic derivative of resistance and resistivity can be used to properly characterize the relative sensitivity of a sensor as a function of temperature, and allows us to directly compare the performance of these sensors as bolometers. Using a logarithmic derivative will also allow for comparing resistance and resistivity directly, which is quite helpful, as for the older chips resistivity is not known.

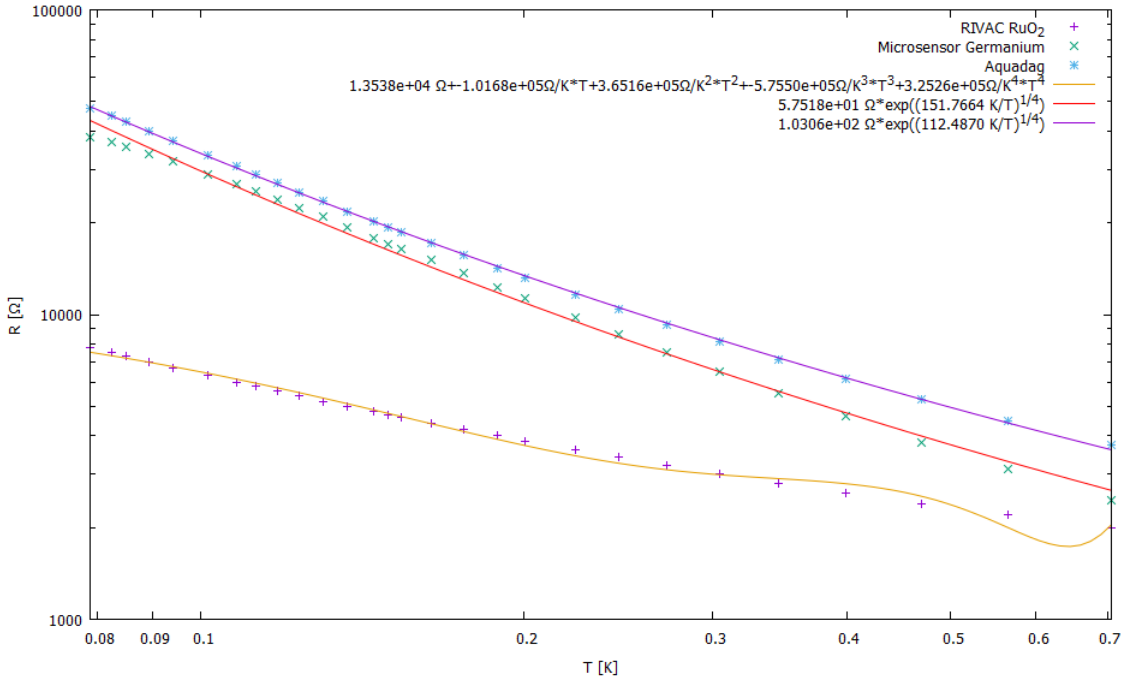

Figure 21: Calibration curves and functions for Aquadag bolometers and the RuO_2 and germanium thermometer chips previously used by Hydrogen Research Group.

To plot the logarithmic derivatives, we need to create calibration functions so we can analytically calculate the derivative functions. For the existing sensors, the germanium and Aquadag sensors can be fitted with a VRH curve as given by eq. (1) using $\beta = \frac{1}{4}$. For the RuO_2 chip we simply used a polynomial fit: $R(T) = a_0 + a_1 T + a_2 T^2 + a_3 T^3 + a_4 T^4$ (see fig. 21). Sample 28 is slightly more difficult, since the kink at around 1 K means a regular fit to eq. (1) is not sufficient. However, we can take the parts which are (almost) linear in a log-log plot, and individually plot to these data points two VRH functions, one before and one after the kink. For these fits we only include the points which are relatively linear on the log-log plot (see fig. 22). We will end up with two calibration curves, one for $T < 1\,\mathrm{K}$ and one for $1\,\mathrm{K} < T < 7\,\mathrm{K}$. For the range below 1 K, we fully expect the linear VRH behaviour to continue, but due to saturation from self-heating, we can merely approximate the expected resistivity by extrapolating the fitted curve to temperatures below the temperature when saturation starts to take effect. As a

result, the results below 0.3 K for our sample 28 are merely an estimate based on this extrapolation, and should be reviewed once the self-heating at low temperatures has been eliminated.

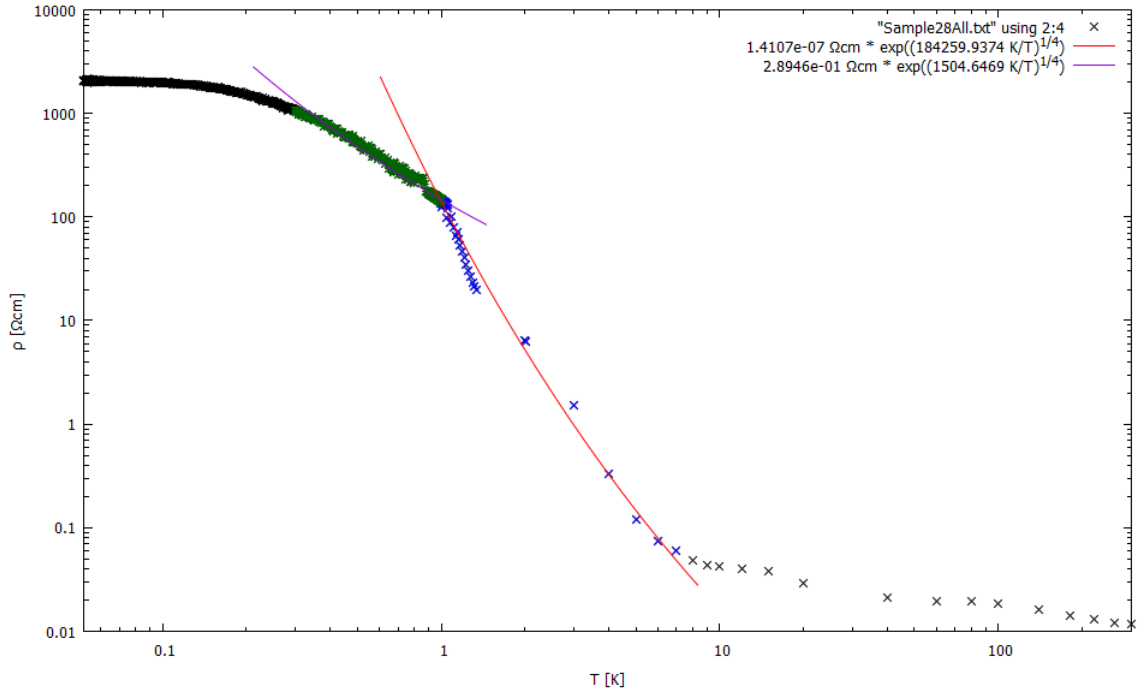

Figure 22: Calibration curves for the linear parts of the silicon sample 28 resistivity measurements. The two linear data sets used for fitting are plotted in green and blue. Data points not used for fits are plotted in black.

We can now use the fitted functions to calculate our logarithmic derivative curves. The curve for silicon sample 28 has a discontinuity at 1 K, when we change from one calibration curve to another at the kink. Additionally, as can be seen from fig. 21, the fit for our RuO_2 chip is rather unstable when going above 0.5 K, and the logarithmic derivative will therefore also be unreliable at higher temperatures. From the logarithmic derivative plot it can clearly be seen that across the entire range the silicon chip is predicted to be more sensitive than any of the other sensors, except for a short range between approximately 0.4 K and 1 K, where ruthenium sensors are shown to be more sensitive.

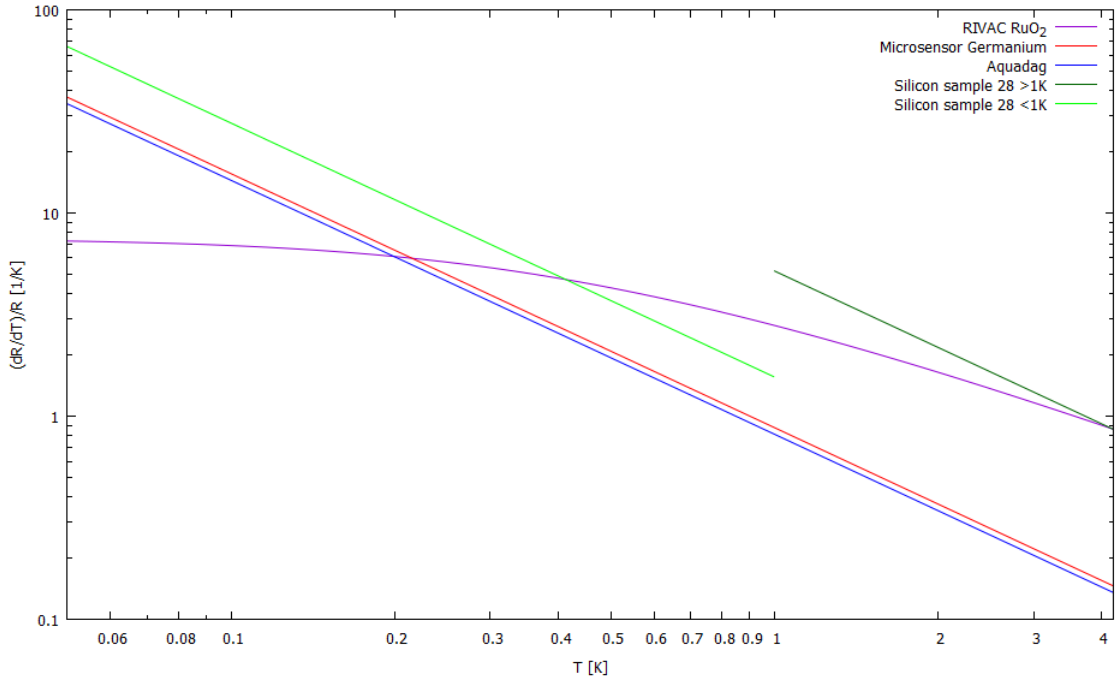

Figure 23: Logarithmic derivative plots from 0.05 K to 4.2 K for RuO_2 and germanium sensors, Aquadag bolometer and the silicon sample 28.

Albeit further measurements are needed to verify that this estimated sensitivity level is indeed correct even at temperatures below 100 mK where the actual hydrogen experiment will take place, these measurements have given a very good argument and proof of concept for the usage of commercially available silicon as a cheap material for high-quality low-temperature bolometers, and we see no obstacle in continuing to develop these bolometers for use as spectroscopy and diagnostic sensors in our hydrogen trap project.

3.6 Improving contacts for silicon chips

Throughout the experiments a problem when working with silicon samples has been creating consistent and high quality electrical contacts. With the bonding wires made of aluminium, the contact resistance usually varied between 150 and 800 ohms, which indicates both high variance in the quality of contacts, and bad overall quality,

as the contact resistance was quite large compared to the overall resistance of the sample at room temperature. While this doesn't prevent us from measuring the resistivity curves as the four-point measurement is mostly unaffected by contact resistance, the high contact resistance means we need to use a higher excitation voltage, which might lead to excess heating at low temperatures and overall worse measurement quality. As such, we will here discuss shortly the possibility of creating better ohmic contacts for our samples.

When trying to create a contact between a metal and a semiconductor, a potential barrier is formed, which is essentially responsible for the contact resistance [45]. The properties of this barrier are heavily dependent on doping, and depending on the height and width of the barrier different processes of carriers passing the barrier may be allowed. Essentially, if the potential barrier is narrow enough to be tunneling-transparent or non-existent, we will be able to form an ohmic contact [46]. The best way to achieve this is to have a very heavy doping concentration locally at the contact.

In our case, we are working with phosphorus-doped silicon (Si:P), so we wish to heavily dope a portion of the surface to form a good metallic contact. As phosphorus is an n-type dopant, we will need to do this heavy doping via some other n-type dopant, such as antimony [47]. As a matter of fact, antimony would be excellent for this due to its low diffusivity, meaning we will not run into the problem of antimony diffusing deep into the silicon and changing its resistivity properties on a large scale, but rather the antimony will stick to the contact site. After this, we can add a layer of another metal that aluminium would be easy to bond to, such as gold. This is a known procedure, where gold-antimony is deposited onto a silicon surface, followed by layers of NiCr and gold [47]. Other potential options include platinum and chromium [48], and titanium [49].

It is also important to consider the method used to create the pad layer. The

easiest methods to use would be sputtering or evaporation, due to relative simplicity and availability of equipment at the University of Turku. Since our main options are the beam evaporator and sputtering systems, we are limited in the available materials. We can use the beam evaporator for making a layer out of gold, platinum or aluminium, and sputtering can be used for at least titanium and chromium. Antimony is slightly more difficult, as albeit it can be easily thermally evaporated, it tends to contaminate any device used for this purpose. The preferable device would be the beam evaporator, as it allows for heat treating and evaporation of several different layers of different materials without exposing the sample to air in between. At this point in time, we haven't yet been able to create proper ohmic contacts to silicon, but further experiments will be made following previous examples [47–49], in order to build higher quality bolometers with proper contacts for wire bonding.

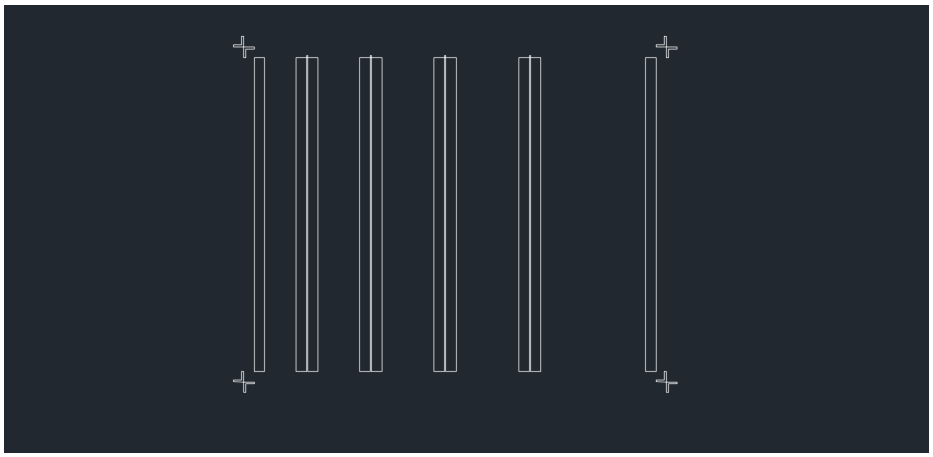

Figure 24: Design of the mask used for creating pads for chips of different sizes. For scale, the rectangular pads are 0.5 mm wide.

To actually make the pads, we will use photolithography to create a mask (fig. 24) at the Aalto Micronova facilities. This mask will be used to etch the pads into a silicon oxide layer on our wafers, so we can later on evaporate our pad material into the etched holes. After making the pads, the wafer should be cut into smaller chips for bolometers.

3.7 Designing the final chip

For the final system we want a silicon chip with a small specific heat and a large surface area for maximum signal. This chip should have pads set up for four-wire measurement, and a substrate that it can be connected to with pads for wire bonding and outside connections. For the connection of the silicon chip to the substrate, there should be a very poor thermal contact of the substrate to the silicon chip, so we can assume the chip to have a stable temperature, and that we can indeed measure the entire energy of the incident, rather than that energy being conveyed out of the chip. On the other hand, the substrate should be well connected to a cold sink so it can cool down the chip after each event. The main thermal link between the chip and the substrate would be the bonding wires.

The substrate can be milled from a regular circuitboard material, leaving stripes for pads. One possible design is shown in fig. 25, with a cross-shaped holder for the silicon chip and four gold stripes for wire pads. The chip should be glued with Stycast, varnish or some other similar adhesive. As an alternative to gluing, the cross piece in the middle could be removed, and the chip could instead be suspended in the middle by thin wires. This would have the advantage that the helium film can flow onto the chip only via these thin wires, leading to a lower maximum total film flow, which makes it far easier to evaporate this film off the bolometer for recombination measurements.

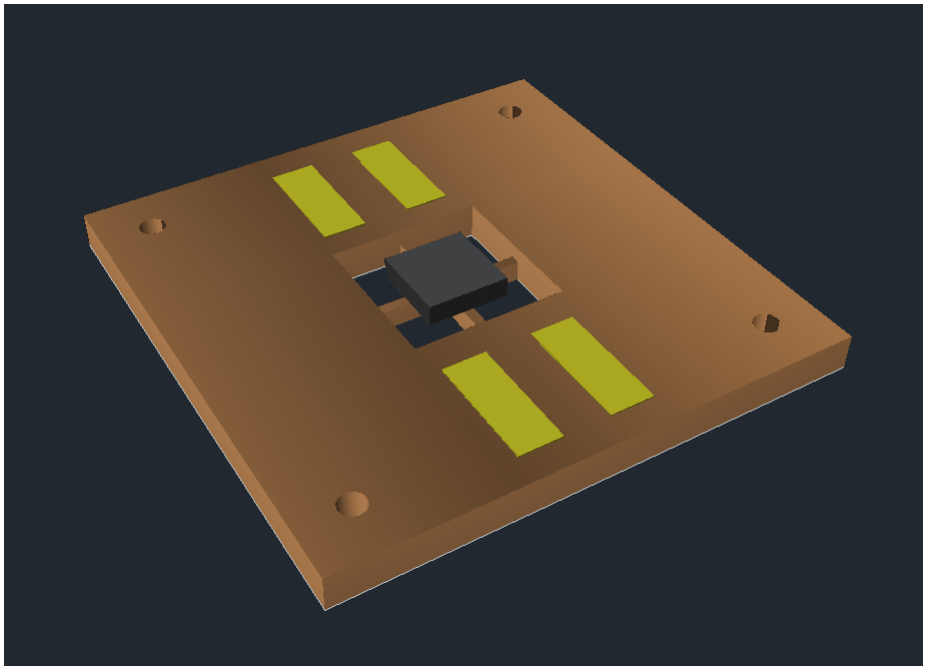

Figure 25: AutoCAD drawing of one of the possible designs for the chips with a cross-shaped holder for the Si sample (black) and four gold pads (yellow) for wire bonding

As we do not yet know exactly what kind of contacts we will be able to make and how large our chips will be, the design is not yet final, albeit it is likely that the design shown in fig. 25 will be quite close to the final design.

4 Conclusions

From our measurements, we can report finding a proper material for building low-temperature bolometers, sample 28 (see fig. 13), that can be predicted to have a better sensitivity than previously used germanium and Aquadag chips by approximately a factor of two below 100 mK.

Additionally, we found that by adjusting the doping concentration, it is possible to change the range of temperature where the optimal sensitivity range of a doped silicon sample is. This finding can be used to create reliable and cheap thermometers for a variety of different temperature ranges.

References

[1] D. E. Pritchard, Phys. Rev. Lett. **51**, 1336 (1983).

[2] D. G. Fried, T. C. Killian, L. Willmann, D. Landhuis, S. C. Moss, D. Kleppner and T. J. Greytak, Phys. Rev. Lett. **81**, 3811 (1998).

[3] J. M. Doyle, J. C. Sandberg, I. A. Yu, C. L. Cesar, D. Kleppner and T. J. Greytak, Phys. Rev. Lett. **67**, 603 (1991).

[4] T. W. Hijmans, J. T. M. Walraven and G. V. Shlyapnikov, Phys. Rev. B **45**, 2561 (1992).

[5] I. F. Silvera and J. Walraven, in the book *Chapter 3: Spin-Polarized Atomic Hydrogen*, Vol. 10 of *Progress in Low Temperature Physics*, editor D. Brewer (Elsevier, 1986), pp. 139 – 370.

[6] S. Vasilyev, E. Tjukanov, M. Mertig and S. Jaakkola, Physica B: Condensed Matter **194-196**, 437 (1994).

[7] H. F. Hess, Phys. Rev. B **34**, 3476 (1986).

[8] J. Luiten, H. Werij, I. Setija, M. Reynolds, T. Hijmans and J. Walraven, Physical review letters **70**, 544 (1993).

[9] C. G. Parthey, A. Matveev, J. Alnis, B. Bernhardt, A. Beyer, R. Holzwarth, A. Maistrou, R. Pohl, K. Predehl, T. Udem and et al., Physical Review Letters **107**, (2011).

[10] R. Mayer, A. Ridner and G. Seidel, Physica B+C **108**, 937 (1981).

[11] B. R. Johnson, J. S. Denker, N. Bigelow, L. P. Lévy, J. H. Freed and D. M. Lee, Phys. Rev. Lett. **52**, 1508 (1984).

[12] L. Willmann and D. Kleppner, in the book *The Hydrogen Atom: Precision Physics of Simple Atomic Systems*, editor S. G. Karshenboim, F. Bassani, F. Pavone, M. Inguscio and T. Hänsch (Springer Berlin HeidelbergBerlin, Heidelberg, 2001), pp. 42–56.

[13] J. JÃ¤rvinen, J. Ahokas and S. Vasiliev, Journal of Low Temperature Physics **147**, (2006).

[14] N. F. Mott, The Philosophical Magazine: A Journal of Theoretical Experimental and Applied Physics **19**, 835 (1969).

[15] N. Mott, Journal of Non-Crystalline Solids **8-10**, 1 (1972).

[16] R. M. Hill, physica status solidi (a) **34**, 601 (1976).

[17] M. H. Cohen, Journal of Non-Crystalline Solids **4**, 391 (1970).

[18] C. H. Seager and G. E. Pike, Phys. Rev. B **10**, 1435 (1974).

[19] A. L. Efros and B. I. Shklovskii, Journal of Physics C: Solid State Physics **8**, L49 (1975).

[20] Y. Meir, Phys. Rev. Lett. **77**, 5265 (1996).

[21] M. Tarasov, J. Svensson, L. Kuzmin and E. E. B. Campbell, Applied Physics Letters **90**, 163503 (2007).

[22] M. Mertig, E. Tjukanov, S. A. Vasilyev, A. Y. Katunin and S. Jaakkola, Journal of Low Temperature Physics **100**, 45 (1995).

[23] O.-A. Adami, L. Rodriguez, V. Reveret, A. Aliane, A. Poglitsch, J.-L. Sauvageot, S. Bounissou, V. Goudon and L. Dussopt, Journal of Low Temperature Physics **193**, 415 (2018).

[24] K. Salonen, Licentiate thesis, University of Turku, Turku, Finland, 1985.

[25] K. Irwin and G. Hilton, in the book *Cryogenic Particle Detection*, editor C. Enss (Springer Berlin HeidelbergBerlin, Heidelberg, 2005), pp. 63–150.

[26] H. Furci, G. Vandoni, A. Macpherson, S. Barriere, A. Castilla, N. Shipman, K. Turaj, M. Wartak and A. Zwozniak, IOP Conference Series: Materials Science and Engineering **502**, 012155 (2019).

[27] B. Dober, D. T. Becker, D. A. Bennett, S. A. Bryan, S. M. Duff, J. D. Gard, J. P. Hays-Wehle, G. C. Hilton, J. Hubmayr, J. A. B. Mates, C. D. Reintsema, L. R. Vale and J. N. Ullom, Applied Physics Letters **111**, 243510 (2017).

[28] S.-F. Lee, J. M. Gildemeister, W. Holmes, A. T. Lee and P. L. Richards, Appl. Opt. **37**, 3391 (1998).

[29] J. Roman, V. Pavlik, K. Flachbart, C. J. Adkins and J. Leib, Journal of Low Temperature Physics **108**, 373 (1997).

[30] K. Flachbart, V. Pavlik, N. Tomasovicova, C. J. Adkins, M. Somora, J. Leib and G. Eska, physica status solidi (b) **205**, 399 (1998).

[31] R. Willekers, F. Mathu, H. Meijer and H. Postma, Cryogenics **30**, 351 (1990).

[32] Q. Li, C. Watson, R. Goodrich, D. Haase and H. Lukefahr, Cryogenics **26**, 467 (1986).

[33] R. Bachmann, H. C. Kirsch and T. H. Geballe, Review of Scientific Instruments **41**, 547 (1970).

[34] M. I. Buraschi, G. U. Pignatel and S. Sanguinetti, Journal of Physics: Condensed Matter **2**, 10011 (1990).

[35] J. K. Wigmore and B. Tlhabologang, Applied Physics Letters **42**, 685 (1983).

[36] F. Tremblay, M. Pepper, D. Ritchie, D. C. Peacock, J. E. F. Frost and G. A. C. Jones, Phys. Rev. B **39**, 8059 (1989).

[37] V. Mitin, P. McDonald, F. Pavese, N. Boltovets, V. Kholevchuk, I. Nemish, V. Basanets, V. Dugaev, P. Sorokin, R. Konakova, E. Venger and E. Mitin, Cryogenics **47**, 474 (2007).

[38] L. J. Neuringer, A. J. Perlman, L. G. Rubin and Y. Shapira, Review of Scientific Instruments **42**, 9 (1971).

[39] C. Boragno, U. Valbusa and G. Pignatel, Applied Physics Letters **50**, 583 (1987).

[40] G. L. Francisco, in the book *Thermosense XXIII*, International Society for Optics and Photonics, editor A. E. Rozlosnik and R. B. Dinwiddie (SPIE, 2001), Vol. 4360, pp. 138 – 148.

[41] T. F. Rosenbaum, R. F. Milligan, G. A. Thomas, P. A. Lee, T. V. Ramakrishnan, R. N. Bhatt, K. DeConde, H. Hess and T. Perry, Phys. Rev. Lett. **47**, 1758 (1981).

[42] A. Aliane, O.-A. Adami, L. Dussopt, L. Rodriguez, W. Rabaud, J.-L. Ouvrier-Buffet, V. Goudon, H. Kaya, C. Vialle, J.-L. Sauvageot, V. Reveret, S. Becker and A. Poglitsch, Journal of Low Temperature Physics **199**, 56 (2020).

[43] K. Lal and G. Bhagavannarayana, Journal of Applied Crystallography **22**, 209 (1989).

[44] W. von Ammon, Nuclear Instruments and Methods in Physics Research Section B: Beam Interactions with Materials and Atoms **63**, 95 (1992).

[45] in the book *Physics of Semiconductor Devices* (John Wiley & Sons, Ltd, 2006), pp. 134–196.

[46] T. V. Blank and Y. A. Gol'dberg, Semiconductors **41**, 1263 (2007).

[47] J. Q. Liu, C. Wang, T. Zhu, W. J. Wu, J. Fan and L. C. Tu, AIP Advances **5**, 117112 (2015).

[48] G. Boberg, L. Stolt, P. A. Tove and H. Norde, Physica Scripta **24**, 405 (1981).

[49] M. Tao, D. Udeshi, S. Agarwal, E. Maldonado and W. Kirk, Solid-State Electronics **48**, 335 (2004).

A Resistivity of a trapezoid-shaped object and error of rectangular approximation

It is well known, that for a general object, the resistance can be calculated as an integral $\int \frac{\rho}{A}\, dL$ over the object along the path L of the current, with ρ being the (possibly variable) resistivity and A being the cross-sectional area of the current path.

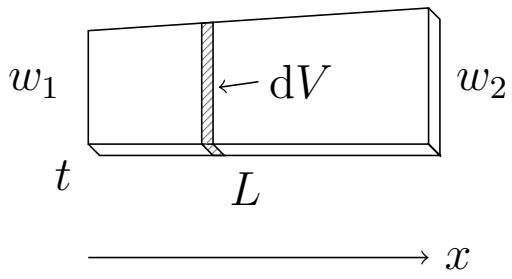

Figure 26: Trapezoid-shaped block, where width of the sample changes linearly from w_1 to w_2 among the length L, while thickness t stays constant. Note differential volume $\mathrm{d}V$ corresponding to a differential resistance $\mathrm{d}R$.

The kind of trapezoidal shape as depicted by Fig 26 is a rather accurate representation of the silicon chips used in PPMS measurements as depicted in section 3.2. For such an object we will set the current to move in the positive x-direction, giving a cross-sectional area of $A = t \cdot w$, with $w = w_1 + \frac{x}{L}(w_2 - w_1)$. We can now integrate over the entire chip (over L):

$$
\begin{aligned}
R &= \int_0^L \frac{\rho}{A}\,\mathrm{d}x \\
&= \int_0^L \frac{\rho}{t\cdot(w_1+\frac{x}{L}(w_2-w_1))}\,\mathrm{d}x \\
&= \frac{\rho}{t}\Bigg|_0^L \ln\left((w_2-w_1)\cdot\frac{x}{L}+w_1\right)\cdot\frac{L}{w_2-w_1} \\
&= \rho\cdot\ln\frac{w_2}{w_1}\cdot\frac{L}{t(w_2-w_1)}
\end{aligned}
$$

$$
\therefore \rho = R\cdot\frac{t(w_2-w_1)}{L\cdot\ln\left(w_2/w_1\right)} \tag{3}
$$

To estimate the error of the rectangular approximation, we can calculate a formula for a rectangular object as the limit of the above formula when $w_2 \Rightarrow w_1$:

$$
\begin{aligned}
\rho_{rect} &= \lim_{w_2\Rightarrow w_1} R\cdot\frac{t(w_2-w_1)}{L\cdot\ln\left(w_2/w_1\right)} \\
&= \lim_{w_2\Rightarrow w_1} R\cdot\frac{t(w_2-w_1)}{L\cdot\ln\left(1+\frac{w_2-w_1}{w_1}\right)} \\
&= R\cdot\frac{t}{L}\frac{w_2-w_1}{\frac{w_2-w_1}{w_1}} \\
&= R\frac{t\cdot w_1}{L} \\
&= R\frac{A}{L}
\end{aligned}
$$

Now we can calculate an estimate for the error of assuming a rectangular shape for a sample by assuming for example that $w_2 = 1.2\cdot w_1$, and seeing how large of a relative error ϵ the rectangular approximation ($w_2 \approx w_1$) causes:

$$\begin{aligned}
\epsilon &= \frac{\rho_{rect} - \rho}{\rho} \\
&= \frac{R\frac{A}{L} - R \cdot \frac{t(w_2 - w_1)}{L \cdot \ln(w_2/w_1)}}{R \cdot \frac{t(w_2 - w_1)}{L \cdot \ln(w_2/w_1)}} \\
&= \frac{w_1 - \frac{0.2 \cdot w_1}{\ln 1.2}}{\frac{0.2 \cdot w_1}{\ln 1.2}} \\
&= \frac{1 - \frac{0.2}{\ln 1.2}}{\frac{0.2}{\ln 1.2}} \approx -8.84\%
\end{aligned}$$

So even for a sample that is quite strongly trapezoidal with 20% variation in width we only get an error of less than 10% for our calculated resistivity. Therefore unless the sample is visibly very badly cut, we can assume that our calculated resistivity is definitely correct within a factor of two, which is more than accurate enough for the purpose of measuring the VRH behaviour of our chips, since we're mostly interested in the rate of change in resistivity as function of temperature, rather than the exact value of the resistivity.